

RSC Advances



This is an *Accepted Manuscript*, which has been through the Royal Society of Chemistry peer review process and has been accepted for publication.

Accepted Manuscripts are published online shortly after acceptance, before technical editing, formatting and proof reading. Using this free service, authors can make their results available to the community, in citable form, before we publish the edited article. This *Accepted Manuscript* will be replaced by the edited, formatted and paginated article as soon as this is available.

You can find more information about *Accepted Manuscripts* in the [Information for Authors](#).

Please note that technical editing may introduce minor changes to the text and/or graphics, which may alter content. The journal's standard [Terms & Conditions](#) and the [Ethical guidelines](#) still apply. In no event shall the Royal Society of Chemistry be held responsible for any errors or omissions in this *Accepted Manuscript* or any consequences arising from the use of any information it contains.

Cite this: DOI: 10.1039/c0xx00000x

www.rsc.org/xxxxxx

ARTICLE TYPE

Photoluminescence phenomena prevailing in *c*-axis oriented intrinsic ZnO thin films prepared by RF magnetron sputtering

Debajyoti Das* and Praloy Mondal

Received (in XXX, XXX) Xth XXXXXXXXXX 20XX, Accepted Xth XXXXXXXXXX 20XX

DOI: 10.1039/b000000x

Substantial *c*-axis orientation of the hexagonal ZnO crystals with wurtzite structure demonstrates only those two preferred peaks in the first-order spectra which are permitted by the Raman scattering selection rule viz., the E_2^{high} and A_1 (LO) modes, that identify the improved structural quality of the undoped ZnO film grown by magnetron sputtering in Ar ambient at an RF power of P= 200 W. Presence of substantial amount of hydroxyl group attached to Zn lattice has been correlated to the dominant *c*-axis orientation of the ZnO crystals which exhibited distinct UV luminescence band that arises due to the typical exciton emission or near-band-edge emission. At higher applied powers, disorder-activated Raman scattering introduces well resolved B_1^{high} mode and gradually growing second order Raman peaks, ($E_2^{high} - E_2^{low}$) and ($B_1^{high} - B_1^{low}$), which are caused by the breakdown of translational symmetry of the lattice by defects or impurities and lead to deviation from preferred *c*-axis orientation with $I_{002}/I_{103} < 1$. Out diffusion of oxygen from the network creates increasing oxygen vacancy states (V_O , V_O^+) and in addition, various other defects e.g., Zn interstitial (Zn_i , Zn_i^+), doubly ionized Zn vacancy (V_{Zn}^{2-}) and oxygen antisite (O_{Zn}) as the dynamic acceptor defects which act as the origins of different visible photoluminescence components classified in the UV-violet, violet, violet-blue, blue and green regions.

Introduction:

ZnO is a $A^{II}B^{VI}$ semiconductor material having hexagonal wurtzite structure. It is nontoxic and abundant in nature; it has high melting point of 2248 K and large bond strength cohesive energy of 1.89 eV. It has a direct and wide band gap (3.37 eV) at room temperature which makes it very attractive material for applications in optical devices such as blue, violet and ultraviolet (UV) light emitting diodes (LEDs) and laser diodes (LDs). The non-stoichiometric undoped ZnO thin films generally exhibits *n*-type conductivity with very high electron densities of about 10^{21} cm^{-3} , controlled by intrinsic defects e.g., oxygen vacancies and zinc interstitials. Although reliable and reproducible high quality *p*-type doping of ZnO is a challenging task, intrinsic *p*-type ZnO has been reported to be produced by adjusting the oxygen partial pressure in the RF magnetron sputtering plasma.¹ Independent control of either Zn or O vacancies in the ZnO network could be a magnificent way in modifying the doping characteristics of the material even in its intrinsic form. By using the high-quality undoped ZnO films, ZnO *p-i-n* homo-junctions have been demonstrated for its use in light-emitting diode (LED) applications.² Actually, there have been some recent advances in the reproducible *p*-type ZnO and ZnO-based light-emitting devices. The *p*-type conductivity has been demonstrated in dual-doped ZnO:(Ag, N) wherein the hole concentration has been identified much higher than that in mono-doped ZnO:Ag or ZnO:N, at the advent of AgZn–N_o type complex acceptors.³ By employing Li–N as a dual-acceptor dopant, *p*-type doping of ZnO

has been realized.⁴ Double hetero-structured light-emitting devices (LEDs) have been fabricated using *p*-Mg_{0.13}Zn_{0.87}O layer or *p*-Mg_{0.25}Zn_{0.75}O:(Li,N) with *n*-ZnO structure, wherein an emission at ~392 nm dominates the emission of the device, which has been attributed to the near-band-edge excitonic emission of ZnO.^{5,6} The *p*-type conductivity has been reported in ZnO platelets synthesized using PCl₅ as a dopant source via aqueous based chemical approach.⁷ Highly ordered ZnO axial *p-n* homojunction containing nanowire via selective in situ lithium (*p*-type) doping of one side of each nanowire has been demonstrated using a low temperature solution-phase synthesis process.⁸

Simultaneous occurrence of low resistivity and high transmittance in the visible spectrum has made zinc oxide thin films useful in a variety of potential applications, such as transparent conducting electrodes for flat panel displays⁹ and solar cells,¹⁰ similar to other transparent conducting semiconductors e.g., tin oxide^{11,12} and tin doped indium oxide.¹³ Short-wave electronic devices, such as blue laser diodes, blue-green light-emitting diodes and ultraviolet detectors, have opened up vast panorama for colour presentation, modern spintronic technology,¹⁴ UV lasers,¹⁵ high-density information storage and gas sensors,¹⁶ etc. The high chemical stability, melting point and large exciton binding energy (60 meV) of ZnO cause it to become a promising UV and blue optoelectronic material. However, their potential for UV devices is impaired because of the reduction of UV luminescence (UVL) yield due to the presence of a large density of unintentional defect states emitting a broad band of

green luminescence (GL).¹⁷ Therefore, it is a challenging task to enhance both the energy and the relative intensity of the UVL emission with respect to the GL emission at the same time.

Some unique optoelectronic properties of direct-gap wurtzite zinc oxide (*w*-ZnO) are comparable and even better than GaN.¹⁸ In particular, ZnO is a brighter emitter than GaN because of its larger exciton energy; it possesses a lower threshold voltage for light-emitting diode (LED) and laser emission, amenability to wet chemical etching, and high radiation resistance. Besides, there are large-area substrates commercially available and the cost for fabrication of ZnO is relatively lower than for III-V nitrides.

In our recent studies we demonstrated the development of transparent and conducting intrinsic ZnO thin films prepared at a high growth rate, by playing on its intrinsic vacancies using the most commonly used RF magnetron sputtering technique. In the present report we intend to explore on its photoluminescent properties correlated to its favoured crystallographic *c*-axis orientation, Raman behaviour, and compositional characteristics, particularly the oxygen vacancies and hydroxyl group attached to Zn lattice, extracted from X-ray photoelectron spectroscopy.

Experimental:

ZnO thin films were prepared onto Corning® Eagle 2000™ rotating glass substrates kept at 300°C, by varying the RF power from 100 to 500 W applied to the high purity (99.99%) undoped ZnO target sputtered by Ar in a RF magnetron sputtering system. The experimental details are given elsewhere.¹⁹ The samples were characterized by X-ray diffraction analysis carried out using a conventional Cu-K_α X-ray radiation ($\lambda \sim 1.5418 \text{ \AA}$) source and Bragg diffraction setup (Seifert 3000P). Raman spectra of the samples were taken from a Renishaw inVia Raman Microscope with an excitation wavelength of 514 nm from an air-cooled Ar⁺ laser source, at a power density of $\sim 2 \text{ mW cm}^{-2}$. The emission spectra of all samples were obtained with FluoroMax-P (HORIBA Jobin Yvon) luminescence spectrophotometer. All the fluorescence spectra were recorded at an excitation wavelength of 370 nm at room temperature. The X-ray photoelectron spectroscopy (XPS) of ZnO film was performed using a focused monochromatized Al-K_α X-ray source (1486.8 eV) in the XPS instrument (Omicron Nano Technology 0571).

Results:

X-Ray Diffraction Studies:

The X-ray diffraction analysis was carried out to investigate the

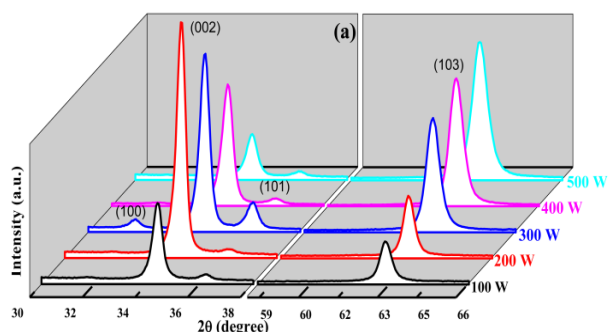


Fig. 1(a) X-ray diffraction spectra of ZnO films prepared by magnetron sputtering at different RF powers varying from 100 to 500 W.

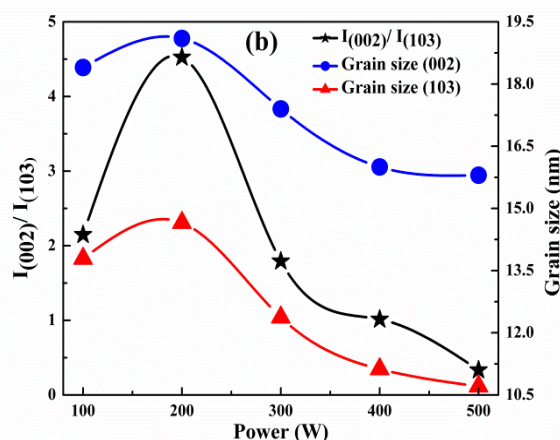


Fig. 1(b) Variations in grain size and changes in the intensity ratio, $I_{(002)}/I_{(103)}$, with applied RF powers.

crystal structures of the ZnO samples. Systematic development of growth along two most prominent crystallographic orientations along (002) and (103) crystallographic planes of ZnO have been demonstrated by the appearance of two corresponding peaks of the XRD spectrum at around $2\theta \sim 34.4^\circ$ and 62.9° , respectively, as shown in Fig. 1(a). It has been identified that the intensity of the (002) peak increased abruptly when applied power *P* increased from 100 to 200 W, while for further increase in *P* the (002) peak systematically reduced in intensity. On the other hand, the (103) peak monotonically increased in intensity with gradual increase in applied RF power from 100 to 500 W.

A significant increase in the intensity ratio of the (002) and (103) peaks, I_{002}/I_{103} , as shown in Fig. 1(b), demonstrates a preferential growth of the material along the $\langle 002 \rangle$ crystallographic orientation, i.e., along the *c*-axis. A very high magnitude of $I_{002}/I_{103} > 4.5$ identifies a substantial *c*-axis orientation of ZnO crystallites grown at *P* = 200 W.²⁰ At RF powers above 400 W, the favoured growth direction gradually shifts from (002) towards the (103) crystallographic plane, as demonstrated by the decaying magnitude of $I_{002}/I_{103} < 1$. The average grain size (*D*), has been estimated from the FWHM (β) of (002) and (103) peaks in the XRD spectra, using Scherer's formula:

$$D = 0.9 \lambda / \beta \cos\theta,$$

that shows a close resemblance in its nature of variation with increasing RF power, as shown in Fig. 1(b). The X-ray diffraction studies identifies a hexagonal wurtzite structure of ZnO films wherein the nanocrystals seem to grow with largest grain size $\sim 19 \text{ nm}$ along (002) orientation i.e., *c*-axis perpendicular to the substrate when prepared at *P* = 200 W.

Raman Study:

Each Zn atom, in the wurtzite structure of ZnO, is tetrahedrally coordinated to four O atoms and vice versa. From the predictions of group theory, the lattice optical phonons at the centre of the Brillouine zone are presented by the following optical symmetry modes:

$$\Gamma = A_1 + 2B_1 + E_1 + 2E_2$$

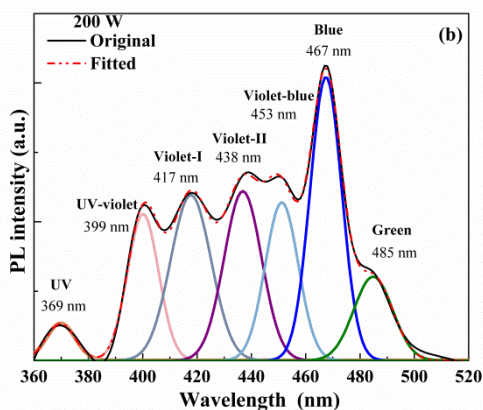


Fig. 3(b). Deconvoluted photoluminescence spectra of the ZnO film prepared at P = 200 W.

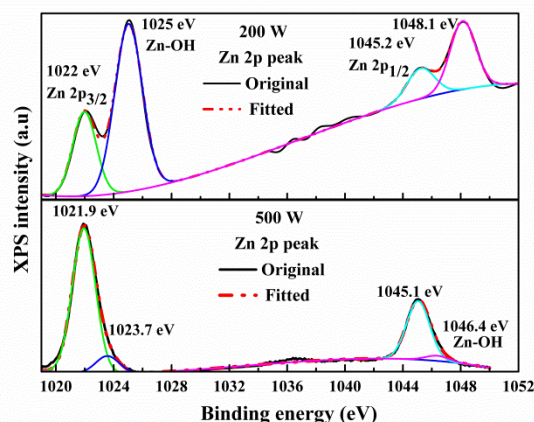


Fig. 4 X-ray photoelectron spectra of the Zn 2p peak of ZnO films prepared at RF powers, P = 200 and 500 W.

been categorised as the UV-violet section at ~399 nm, two violet components viz., violet-I at ~417 nm and violet-II at ~438 nm, violet-blue fragment at ~453 nm, blue emission at ~467 nm and a green emission around ~500 nm with a span over 480–520 nm. The UV luminescence bands in the ZnO films depend strongly on surface band bending and those are created from recombination of bound excitons (BEs) complex located near the surface and grain boundaries within the films. There are two factors which directly affect the UV emission in ZnO films. One is the DLE (deep level emission) recombination centres and the other is the non-radiative recombination centres that can degrade the UV emission.

The UV emission at ~369 nm that identifies typical exciton emission or near-band-edge emission, is most prominent at an optimum RF power of 200 W, demonstrating better crystalline quality of the sample that has been recognized by its dominant *c*-axis orientation, as identified by XRD studies.

However, on increase in RF power, the visible emission that has mostly the defect origin is becoming proportionally significant. The intensity of the visible emission band is, in general, much higher than that of the exciton emission band. Conversely, the intensity under visible band increases when the other band reduces, indicating both emission processes to compete with each other. At elevated RF powers, out diffusion of oxygen from the ZnO network creates enough oxygen vacancies, demonstrating prominent green emission in photoluminescence. However, in order to account for the systematic relative increase in intensity of different components in the visible region, change in the chemical composition of the material at elevated RF power could be a significant parameter.

X-Ray Photoelectron Spectroscopy:

XPS survey spectra were first produced before the high-resolution scan for O and Zn. The binding energies were calibrated with respect to the C1s peak at 284.6 eV. The deconvolutions of the XPS spectrum for core level Zn 2p_{3/2} of ZnO film prepared at P = 200 W are represented in Fig. 4. A good fit to the experimental data is obtained with two deconvoluted Gaussian components. Shift in the binding energy towards above 1021 eV rules out the presence of elemental Zn in ZnO film. The observed peak at the binding energy of 1022 eV is associated to Zn 2p_{3/2} species in stoichiometric ZnO. The other peak present at

higher binding energy of 1025 eV originates from the –OH groups attached to Zn ions on the surface of the films and/or the Zn deficient regions (V_{Zn}).²⁹ The core level Zn 2p_{1/2} XPS spectrum of the film produced two satellite Gaussian components at 1045.2 and 1048.1 eV which correspond to the Zn 2p_{1/2} species in ZnO matrix and the –OH contaminants attached to Zn ions. An energy separation of 23.2 eV between two core level Zn 2p components makes out a good agreement with the literature values for ZnO.^{30,31} However, in case of the film prepared at P = 500 W, the Zn 2p spectrum possess two isolated symmetric Gaussian components corresponding to Zn 2p_{3/2} species at 1022 eV and Zn 2p_{1/2} species at 1045.2 eV, which are at exactly identical energies for similar components for earlier sample. The nature of distribution of the Zn 2p spectral components indicate that the chemical valence of Zn at the surface of ZnO is at (+2) oxidation state for this film.³² It is found from Fig. 5 that O1s core level peaks of the films have asymmetric shapes which could be fitted by three nearly Gaussian peaks, centered at ~529.7, ~530.5 and ~532.3 eV, for the films prepared at P = 200 W, and ~529.9, ~530.6 and ~532.2 eV, for P = 500 W. Among the three well identified Gaussian components, the lower two binding energy components are identified as due to two types of O²⁻ ions, namely O_I and O_{II}, while the third component appearing at

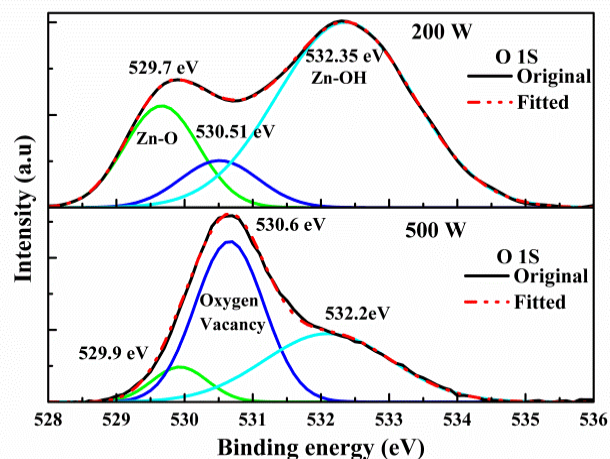


Fig. 5 X-ray photoelectron spectra of the O 1s peak of ZnO films prepared at RF powers P = 200 and 500 W.

highest binding energy at ~ 532.3 eV is attributed to the presence of –OH bonds attached to Zn ions on the surface of the films.³³ Such a double oxygen 1s peak was common for oxides containing cations in multiple valence states. It was suggested that the O_I²⁻ ions had neighboring atoms with their full complement of six nearest neighbor O²⁻ ions in the ZnO lattice i.e., the wurtzite structure of ZnO,³⁴ and that the O_{II}²⁻ ions were in oxygen-deficient regions within the matrix of ZnO.³⁵ Therefore, the changes in the relative intensity of O_{II}/O_I were connected to the variations in the concentration of oxygen vacancies. The relative intensity of O_{II}/O_I has been found to increase significantly from ~ 0.5 to 5.7 for increasing the applied RF power from 200 to 500 W which identifies the formation of a considerable amount of oxygen vacancies in the ZnO network due to high electrical excitation of the sputtered atoms. Careful observation on the XPS O 1s and Zn 2p spectra demonstrates that increasing RF power applied to the sputtering target leads to the growth of ZnO films wherein the chemisorbed oxygen desorbs from the film surface and the oxygen vacant states increases within Zn lattice interstitials.

Discussion:

The XRD pattern revealed that the as-deposited ZnO films were polycrystalline with a hexagonal structure, and had a preferred orientation with the *c*-axis perpendicular to the substrate. The (002) diffraction angle was close to that of the standard ZnO crystal (34.421, JCPDF#36-1451), and no metallic Zn characteristic peak or no characteristic peaks of other impurities was observed in the pattern. Beside the (002), (103) diffraction peak increased uninterruptedly, whose relative intensity $I_{(103)}/I_{(002)}$ increased monotonously as the applied RF power increased systematically beyond 200 W.

Presence of increased hydroxyl group attached to Zn lattice, as revealed by XPS studies, could be correlated to the dominant *c*-axis orientation at P= 200 W, corresponding to distinct UV luminescence exhibited by the material. While the increased oxygen vacancy at higher powers keeps on favouring the growth along (103) crystallographic orientation which might be correlated to increased visible emission, particularly the luminescence in green and violet region.

When the incident light is parallel to the *c*-axis of ZnO samples, the Raman active E_2 modes and $A_1(LO)$ modes are allowed, whereas $A_1(TO)$ and $E_1(TO)$ modes are forbidden, according to Raman selection rules.³⁶ In case of the present Raman measurement, the incident light is exactly perpendicular to the samples surface. For the present set of samples, in general, the E_2^{high} and $A_1(LO)$ modes are distinctly present in the Raman spectrum which identifies that ZnO films are of fairly Wurtzite structure. In addition, the complete absence of any other accompanying Raman band demonstrates the most favoured *c*-axis orientation of the hexagonal ZnO crystalline structures prepared at an optimum RF power, P = 200 W, applied to the sputtering target, which has been equitably supported by the results e.g., a very high magnitude of $I_{002}/I_{103} > 4.5$, obtained from X-ray diffraction studies.

The luminescence emission properties are extremely sensitive to the defect states in ZnO. Emissions in the visible range (violet,

blue, green, yellow, and orange-red) are likely due to donor acceptor transitions involving the point defects such as vacancies of oxygen and zinc, interstitial oxygen and zinc, antisite oxygen, as well as other extrinsic impurities in ZnO.³⁷ In spite of many investigations on the luminescent properties a consensus about the origins of defect-related visible emissions has not been reached due to the complexity of the microscopic details. The yellow emission is usually unstable on thermal treatment³⁸ and is typically attributed to interstitial oxygen^{39,40} and absorbed hydroxyl group.^{41,42} The orange-red emission observed in air annealed ZnO nanostructures has been assigned to excess oxygen and interstitial zinc.⁴³ In case of ZnO nanoparticles, green emission is often believed to be stemming from the surface.⁴⁴ Presence of surface complexes e.g., physically adsorbed hydroxyl groups attached to the ZnO nanoparticles have pronounced effect on the origin of green luminescence.⁴⁵ Furthermore, green emission is attributed to the singly ionized oxygen vacancy (Vo^+) which can act as deep level electron donor states, or surface defects.^{46,47} According to many theoretical calculations and experimental results,^{48,49} only interstitial zinc (Zn_i) among the point defects in the ZnO lattice is a shallow donor and the corresponding level is located slightly below the conduction band-edge.

The XPS results revealed the as-grown films as non-stoichiometric which can contain many defects in the lattice or the surface. The UV emission is associated to the excitonic recombination corresponding to the near band-edge transition, whereas the visible emission band is commonly attributed to the defects on the surface or in the bulk of the material. Increasing concentration of defects in the films prepared at higher RF powers could result in the decrease of UV emission and the enhancement of defect emission band in the visible region. The weak UV emission and strong visible emission band in PL spectra for the material grown at high power at P = 500 W is consistent with its increasing oxygen vacancies which might have stronger influence than the reducing hydroxyl group attached to Zn lattice.

In most cases, the photoluminescence (PL) of ZnO nanoparticles has two components. A relatively weak and narrow UV emission band is observed around 370 nm (3.35 eV), just below the onset of absorption. This band arises due to the typical exciton emission or near-band-edge emission, i.e., photo-generated electron recombination with holes in the valence band or in traps near the valence band, considering the band gap of ZnO to be ~ 3.37 eV. The radiative lifetime of excitons in pure ZnO lies in the sub-nanosecond range.⁵⁰ A much stronger and broader emission band arises in the visible spectrum. In contrast to the exciton emission, the lifetime of the visible emission is much longer, viz. in the μs range.⁵¹ This excitonic emission is directly linked to confinement effects and, consequently, depends on the size of the nanoparticles. For ZnO, such a confinement effect can be observed only for sizes below 10 nm.³⁸ In the samples discussed herein the excitonic emission has been found near 370 nm (~3.35 eV) and the confinement effects are not expected, the estimated size of ZnO nanoparticles in the films being always above 10 nm. The intensity of the visible emission band is much higher than that of the exciton emission band. However, the intensity under visible band increases when the

other band reduces, as both emission processes compete with each other.

The visible emission process involves efficient trapping of photogenerated holes somewhere in the particle. The rate of this hole trapping must be much faster than the radiative recombination rate of the exciton emission. Because of the large surface-to-volume ratio of ZnO particles, efficient and fast trapping of photogenerated holes at surface sites can be expected. A probable candidate for the trapping of holes is O^{2-} ions at the surface.⁵² The rate for a surface trapping process decreases as the particle size increases since the surface-to-bulk ratio decreases. The transition rate of the exciton recombination will not be influenced strongly by the particle size and thus the relative intensity of the exciton emission will increase with increasing particle size, as observed in case of ZnO film prepared at $P=200$ W.

Van Dijken et al. have explained the phenomenon at the origin of green emission around 500 nm by the recombination of a shallowly trapped electron with a deeply trapped hole.⁵³ In this scheme, the photogenerated hole is first trapped at the surface of the nanoparticles by surface defects such as O^{2-}/O^- and then migrates to vacancy levels located deep in the particle leading to the formation of a deep hole trapped level above the valence band. The emission around 500 nm (~ 2.48 eV) occurs when the photogenerated hole trapped in the deep oxygen vacancy recombines with the photogenerated electron trapped in a shallow level located just below the conduction band.

Regarding the origin of the blue emission from ZnO QDs a number of hypotheses have been proposed, such as electron transition from oxygen vacancies (V_O) to the valence band,⁵⁴ zinc interstitials (Zn_i) to zinc vacancies (V_{Zn}),⁵⁵ Zn_i to the valence band⁵⁶ or OH- groups at the surface of the particles⁵⁷ which mostly vary with the synthesis techniques. In a recent investigation on the blue emission from ZnO QDs synthesized by a sol-gel method Han *et al*⁵⁸ found that ZnO QDs with blue emission can be obtained only in the presence of Li^+ cations and excessive OH^- anions, and interstitial oxygen defects (O_i) are determined as the origin of the blue emission. The long lifetime obtained from PL decay profiles strongly identified the blue emission originating from a de-excitation process related to defect states.^{59,60} Furthermore, blue-emission with an average lifetime of ~ 169 ns from ZnO QDs with size larger than those of green-emission ones with an average lifetime of 256 ns, discarded any possibility of its origin from the blue shift of the green emission as a consequence of quantum confinement effect.

The excessive OH^- ions cause a stoichiometric excess of oxygen in ZnO QDs, which favours the formation of specific defects, including interstitial oxygen (O_i), oxygen antisite (O_{Zn}) and zinc vacancies (V_{Zn}^0 , V_{Zn}^- , V_{Zn}^{2-}).⁶¹ As all of the above defects are acceptors in nature and an acceptor-to-acceptor transition is forbidden, the only possible transition path for the blue emission happens to be from the conduction band to an acceptor. For ZnO bulk material, energy levels of O_i , O_{Zn} , V_{Zn}^0 , V_{Zn}^- and V_{Zn}^{2-} are 3.06, 2.66, 0.56, 2.28 and 2.38 eV below the conduction band, respectively.⁵⁸ For the present set of ZnO samples a narrow and very sharp blue luminescence peak appears exactly at 2.66 eV (~ 467 nm) which identifies oxygen antisite (O_{Zn}) as the responsible defects. Although the formation energy

of O_{Zn} is very high in Zn-rich environment, it reduces substantially in O-rich ZnO network.⁶² Oxygen antisites could potentially be created under non-equilibrium conditions such as under irradiation or ion implantation which is highly probable in case of formation of ZnO films during magnetron sputtering at sufficiently high RF power ~ 200 W or above.

However, at very high RF power, $P \sim 500$ W, ZnO system deviates from its O-rich state due to out-diffusion of O from the network. Accordingly, the formation energy of O_{Zn} increases substantially and defects with high formation energies will occur in low concentrations, thereby reducing the blue PL intensity. Simultaneously, Zn_i defects increases significantly at higher P because of its grossly reduced formation energy.⁶² Increasing Zn_i defects introduces enhanced violet emission which has been attributed to electron-hole recombination between Zn_i defects level and the valence band.⁶³ Using full-potential linear muffin-tin orbital method, Sun⁶⁴ calculated the energy levels of the intrinsic defects in undoped ZnO films and identified interstitial zinc (Zn_i) defect levels at 2.90 eV (~ 428 nm) away from the valence band which lies exactly at the middle of violet spectrum of PL identified in our samples. Systematic increase in the intensity of the violet PL relative to that of blue PL at increasing applied RF power beyond 200 W is evident from Fig. 3(a).

The visible emission over a wide energy range around 380–460 nm could be nicely deconvoluted into four satellite components in each case, as shown in Fig. 3(b). Analysis on the possible origin of individual component has been made from the available energy positions of various defect centres existing within Zn–O system.^{65,66} An UV-violet emission luminescence peak at 399 nm (3.10 eV) could be attributed to possible electron transition from the conduction band to single ionized oxygen vacancy (V_O^+) as the responsible acceptor defects located at 0.27 eV above the valence band. Two satellite components of the violet luminescence are observable in each spectrum. The violet-I luminescence peak at 417 nm (2.96 eV) is occurring through possible transition of electrons trapped at Zn interstitial (Zn_i) defects to the valence band, while the violet-II luminescence peak at 438 nm (2.83 eV) arises through possible electron transition between ionized Zn interstitial (Zn_i^+) defects level and the valence band. Radiative recombination of electrons from the doubly ionized Zn vacancy (V_{Zn}^{2-}) to holes in the valence band leads to the evolution of violet-blue component of PL peak located at around 450 nm. At higher RF power, out diffusion of oxygen from the network increases oxygen vacancies (V_O , V_O^+) thereby enhancing PL intensities of green and UV-violet components, increasing Zn interstitial defects (Zn_i , Zn_i^+) enhances the violet (I & II) components, while the simultaneous reduction of Zn vacancy (V_{Zn}^{2-}) systematically reduces the violet-blue to violet intensity ratio, as evident from careful observation in Fig. 3(a).

The photo excitation and the emission phenomena in the present scenario can then be summarized as follows, along with a schematic presentation in Fig. 6:

- i) A relatively weak and narrow UV emission band around 370 nm (~ 3.35 eV) arising due to the typical exciton emission or near-band-edge emission, i.e., photo-generated electron recombination with holes in the valence band or in traps near the valence band.

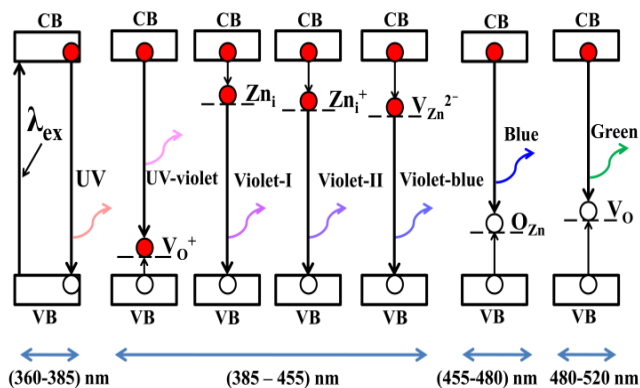


Fig. 6 Schematic band diagram, demonstrating various PL emission components originated due to electronic transitions between different defect levels and the band edges of ZnO films, prepared by RF magnetron sputtering system.

ii) An UV-violet emission peak at 399 nm (~ 3.10 eV) attributed to possible electron transition from the conduction band to single ionized oxygen vacancy (V_{O^+}) as the responsible acceptor defects located at 0.27 eV above the valence band.

iii) The violet-I luminescence peak at 417 nm (~ 2.96 eV) appearing through possible transition of electrons trapped at Zn interstitial (Zn_i) defects to the valence band.

iv) The violet-II luminescence peak at 438 nm (~ 2.83 eV) arises due to electron transition between ionized Zn interstitial (Zn_i^+) defects level and the valence band.

v) Radiative recombination of electrons from the doubly ionized Zn vacancy (V_{Zn}^{2-}) to holes in the valence band leads to the evolution of violet-blue component of PL peak located at around 450 nm (~ 2.75 eV).

vi) A narrow and very sharp blue luminescence peak appearing at 467 nm (~ 2.66 eV), occur through potential electron transition from the conduction band to oxygen antisite (O_{Zn}) as the responsible acceptor defects.

vii) An emission band around 500 nm (~ 2.48 eV) arising when the photogenerated holes trapped in the deep level oxygen vacancy (V_O) recombine with the electrons trapped in a shallow level located just below the conduction band.

Conclusion:

Among the possible Raman-active phonon modes in the hexagonal ZnO crystal with wurtzite structure, the appearance of only those two preferred peaks in the first-order spectra which are permitted by the Raman scattering selection rule viz., the E_2^{high} and A_1 (LO) modes, identify the improved structural quality of the undoped ZnO film grown at P= 200 W of RF power. A_1 (LO) mode appears only when the c -axis of wurtzite ZnO remains parallel to the incident light. The backscattering Raman spectra for highly c -axis oriented ZnO thin films do possess E_2^{high} mode, as well. Substantial c -axis orientation of the ZnO crystals prepared at P= 200 W identified from XRD studies corroborates the Raman observations. At higher applied powers, disorder-activated Raman scattering introduces well resolved B_1^{high} mode and gradually growing second order Raman peaks, ($E_2^{high} - E_2^{low}$)

and ($B_1^{high} - B_1^{low}$), which are caused by the breakdown of translational symmetry of the lattice by defects or impurities and lead to ZnO wurtzite structure deviated from preferred c -axis orientation with $I_{002}/I_{103} < 1$.

The XPS results revealed the as-grown films as non-stoichiometric which can contain many defects in the lattice or the surface. Presence of substantial amount of hydroxyl group attached to Zn lattice, at P= 200 W, could be correlated to the dominant c -axis orientation of the ZnO crystals which exhibited distinct UV luminescence band that arises as a result of the typical exciton emission or near-band-edge emission, i.e., due to recombination of photo-generated electrons with holes in the valence band or in traps near the valence band. With the increase in applied RF power out diffusion of oxygen from the network creates considerable volume of oxygen vacancy which induces on favouring the growth along (103) crystallographic orientation. In addition to increasing oxygen vacancies in neutral (V_O) and ionized (V_{O^+}) states, a number of other defects are generated, which include Zn interstitial (Zn_i , Zn_i^+), doubly ionized Zn vacancy (V_{Zn}^{2-}) and oxygen antisite (O_{Zn}) as the dynamic acceptor defects which act as the defect origins of different visible photoluminescence components classified in the UV-violet, violet, violet-blue, blue and green regions. The origin and the evolution of photoluminescence in the UV and various visible segments have been schematically demonstrated.

Acknowledgement:

The work has been done under nano-silicon projects funded by Department of Science and Technology (Nano-Mission Program) and Council of Scientific and Industrial Research, Government of India. The XPS studies have been performed using facilities of DST Unit on Nano-Science at IACS.

Notes

Nano-Science Group, Energy Research Unit, Indian Association for the Cultivation of Science, Jadavpur, Kolkata – 700 032, India. E-mail (D. Das): erdd@iacs.res.in ; Fax: +91(33)24732805

References

- G. Xiong, J. Wilkinson, B. Mischuck, S. Tüzemen, K. B. Ucer and R. T. Williams, *Appl. Phys. Lett.*, 2002, **80**, 1195–1197.
- A. Tsukazaki, A. Ohtomo, T. Onuma, M. Ohtani, T. Makino, M. Sumiya, K. Ohtani, S. F. Chichibu, S. Fuke, Y. Segawa, H. Ohno, H. Koinuma and M. Kawasaki, *Nature Mater.*, 2005, **4**, 42–46.
- L. Duan, P. Wang, X. Yu, X. Han, Y. Chen, P. Zhao, D. Lia and R. Yaob, *Phys. Chem. Chem. Phys.*, 2014, **16**, 4092–4097.
- F. Sun, C. X. Shan, B. H. Li, Z. Z. Zhang, D. Z. Shen, Z. Y. Zhang and D. Fan, *Optics Lett.*, 2011, **36**, 499–501.
- Y. J. Lu, C. X. Shan, M. M. Jiang, B. H. Li, K. W. Liu, R. G. Lic and D. Z. Shen, *RSC Adv.*, 2014, **4**, 16578–16582.
- J. S. Liu, C. X. Shan, H. Shen, B. H. Li, Z. Z. Zhang, L. Liu, L. G. Zhang and D. Z. Shen, *Appl. Phys. Lett.*, 2012, **101**, 011106.
- B. Panigrahy and D. Bahadur, *RSC Adv.*, 2012, **2**, 6222–6227.
- G. Li, A. Sundararajan, A. Mouti, Y. J. Chang, A. R. Lupini, S. J. Pennycook, D. R. Strachan and B. S. Guiton, *Nanoscale*, 2013, **5**, 2259–2263.
- T. Minami, *Semicond. Sci. Technol.*, 2005, **20**, S35–S44.
- T. Shinagawa, K. Shibata, O. Shimomura, M. Chigane, R. Nomura and M. Izaki, *J. Mater. Chem. C*, 2014, **2**, 2908–2917.
- D. Das and R. Banerjee, *Thin Solid Films*, 1987, **147**, 321–331.

- 12 R. Banerjee and D. Das, *Thin Solid Films*, 1987, **149**, 291–301.
- 13 R. Banerjee, D. Das, S. Ray, A. K. Batabyal and A. K. Barua, *Solar Energy Materials*, 1986, **13**, 11–23.
- 14 I. Z'utic, J. Fabrian and S. S. Das, *Rev. Mod. Phys.* 2004, **76**, 323–410.
- 15 A. B. Djuris'ic, X. Chen, Y. H. Leung and A. M. C. Ng, *J. Mater. Chem.*, 2012, **22**, 6526–6535.
- 16 B. Liu, Z. Wang, Y. Dong, Y. Zhu, Y. Gong, S. Ran, Z. Liu, J. Xu, Z. Xie, D. Chen and G. Shen, *J. Mater. Chem.*, 2012, **22**, 9379–9384.
- 17 X. Peng, L. Manna, W. Yang, J. Wickham, E. Scher, A. Kadavanich and A. P. Alivisatos, *Nature*, 2000, **404**, 59–61.
- 18 Ü. Özgür, Ya. I. Alivov, C. Liu, A. Teke, M. A. Reshchikov, S. Doğan, V. Avrutin, S. J. Cho and H. Morkoç, *J. Appl. Phys.*, 2005, **98**, 041301.
- 19 P. Mondal and D. Das *Appl. Surf. Sci.*, 2013, **286**, 397–404.
- 20 X. Li, Y. Wang, W. Liu, G. Jiang and C. Zhu, *Materials Letters*, 2012, **85**, 25–28.
- 21 T. C. Damen, S. P. S. Porto, and B. Tell, *Phys. Rev.*, 1966, **142**, 570–574.
- 22 A. Arguello, D. L. Rousseau and S. P. S. Porto, *Phys. Rev.*, 1969, **181**, 1351–1363.
- 23 J. Serrano, A. H. Romero, F. J. Manjón, R. Lauck, M. Cardona and A. Rubio, *Phys. Rev. B*, 2004, **69**, 094306.
- 24 R. Cusco, E. A. Llado, J. Ibanez, L. Artus, J. Jimenez, B. Wang and M. J. Callahan, *Phys. Rev. B*, 2007, **75**, 165202.
- 25 F. J. Manjón, B. Marí, J. Serrano and A. H. Romero, *J. Appl. Phys.*, 2005, **97**, 053516.
- 26 M. Tzolov, N. Tzenov, D. Dimova-Malinovska, M. Kalitzova, C. Pizzuto, G. Vitali, G. Zollo and I. Ivanov, *Thin Solid Films*, 2000, **379**, 28–36; 2001, **396**, 274–281.
- 27 L. Du, Z. B. Gu, M. H. Lu, J. Wang, S. T. Zhang, J. Zhao, G. X. Cheng, H. Heng and Y. F. Chen, *J. Appl. Phys.*, 2006, **99**, 123515.
- 28 J. F. Scott, *Phys. Rev. B*, 1970, **2**, 1209–1211.
- 29 G. Deroubaix and P. Marcus, *Surf. Interface Anal.*, 1992, **18**, 39–46.
- 30 J. F. Moulder, W. F. Stickle, P. E. Sobol and K. D. Bomben, *Handbook of X-ray Photoelectron Spectroscopy*, Perkin-Elmer Corporation, Eden Prairie, 1992.
- 31 C. D. Wagner, A. V. Naumkin, A. Kraut-Vass, J. W. Allison, C. J. Powell and J. R. J. Rumble, NIST X-ray Photoelectron Spectroscopy Database, Default.aspx, (accessed November 2012) U.S. Secretary of Commerce, 2007
- 32 Y. W. Ma, J. Ding, J. B. Yi, H. T. Zhang and C. M. Ng, *J. Appl. Phys.*, 2009, **105**, 07C503.
- 33 E. De la Rosa, S. Sepulveda-Guzman, B. Rejea-Jayan, A. Torres, P. Salas, N. Elizondo and M. J. Yacamán, *J. Phys. Chem. C*, 2007, **111**, 8489–8489.
- 34 N. S. Ramgir, D. J. Late, A. B. Bhise, M. A. More, I. S. Mulla, D. S. Joag and K. Vijayamohanan, *J. Phys. Chem. B*, 2006, **110**, 18236–18242.
- 35 Fan J. J. C and Goodenough J. B, *J. Appl. Phys.*, 1977, **48**, 3524–3531.
- 36 L. L. Yang, Q. X. Zhao, M. Willander, J. H. Yang and I. Ivanov, *J. Appl. Phys.*, 2009, **105**, 053503.
- 37 M. D. McCluskey and S. J. Jokela, *J. Appl. Phys.*, 2009, **106**, 071101.
- 38 A. B. Djuris'ic and Y. H. Leung, *Small*, 2006, **2**, 944–961.
- 39 L. P. Li, X. Q. Qiu and G. S. Li, *Appl. Phys. Lett.*, 2005, **87**, 124101.
- 40 X. L. Wu, G. G. Siu, C. L. Fu and H. C. Ong, *Appl. Phys. Lett.*, 2001 **78**, 2285–2287.
- 41 A. B. Djuris'ic, Y. H. Leung, K. H. Tam, Y. F. Hsu, L. Ding, W. K. Ge, Y. C. Zhong, K. S. Wong, W. K. Chan, H. L. Tam, K. W. Cheah, W. M. Kwok and D. L. Phillips, *Nanotechnology*, 2007, **18**, 095702.
- 42 J. J. Qiu, X. M. Li, W. Z. He, S. J. Park, H. K. Kim, Y. H. Hwang, J. H. Lee and Y. D. Kim, *Nanotechnology*, 2009, **20**, 155603.
- 43 J. P. Liu, C. X. Xu, G. P. Zhu, X. Li, Y. P. Cui, Y. Yang and X. W. Sun, *J. Phys. D: Appl. Phys.*, 2007, **40**, 1906–1909.
- 44 H. Zhou, H. Alves, D. K. Hoffmann, W. Kriegseis, B. K. Meyer, G. Kaczmarczyk and A. Hoffmann, *Appl. Phys. Lett.*, 2002, **80**, 210–212.
- 45 A. Sharma, B. P. Singh, S. Dhar, A. Gondorf and M. Spasova, *Surface Science*, 2012, **606**, L13–L17.
- 46 M. K. Patra, K. Manzoor, M. Manoth, S. R. Vadera and N. Kumar, *J. Lumin.*, 2008, **128**, 267–272.
- 47 S. Shi, J. Xu, X. Zhang and L. Li, *J. Appl. Phys.*, 2011, **109**, 103508.
- 48 H. B. Zeng, G. T. Duan, Y. Li, S. K. Yang, X. X. Xu and W. P. Cai, *Adv. Funct. Mater.*, 2010, **20**, 561–572.
- 49 D. C. Look, J. W. Hemsky and J. R. Sizelove, *Phys. Rev. Lett.*, 1999, **82**, 2552–2554.
- 50 V. V. Travnikov, A. Freiberg and S. F. Savikhin, *J. Lumin.*, 1990, **47**, 107–112.
- 51 M. Anpo and Y. Kubokawa, *J. Phys. Chem.*, 1984, **88**, 5556–5560.
- 52 G. H. Schoenmakers, D. Vanmaekelbergh and J. J. Kelly, *J. Phys. Chem.*, 1996, **100**, 3215–3220.
- 53 A. van Dijken, E. A. Meulenlamp, D. Vanmaekelbergh and A. Meijerink, *J. Phys. Chem. B*, 2000, **104**, 1715–1723.
- 54 L. Zhang, Y. Longwei, C. Wang, N. Lun, Y. Qi and D. Xiang, *J. Phys. Chem. C*, 2010, **114**, 9651–9658.
- 55 C. H. Ahn, Y. Y. Kim, D. C. Kim, S. K. Mohanta and H. K. Cho, *J. Appl. Phys.*, 2009, **105**, 013502.
- 56 M. Abdullah, I. W. Lenggoro, K. Okuyama and G. S. Frank, *J. Phys. Chem. B*, 2003, **107**, 1957–1961.
- 57 S. Monticone, R. Tufeu and A. V. Kanaev, *J. Phys. Chem. B*, 1998, **102**, 2854–2862.
- 58 L. L. Han, L. Cui, W. H. Wang, J. L. Wang and X. W. Du, *Semicond. Sci. Technol.*, 2012, **27**, 065020.
- 59 W. J. Qin, J. Sun, J. Yang and X. W. Du, *Mater. Chem. Phys.*, 2011, **130**, 425–430.
- 60 A. G. Joshi, S. Sahai, N. Gandhi, Y. G. Radha Krishna and D. Haranath, *Appl. Phys. Lett.* 2010, **96**, 123102.
- 61 C. B. Tay, S. J. Chua and K. P. Loh, *J. Cryst. Growth*, 2009, **311**, 1278–1284.
- 62 A. Janotti and C. G. Van de Walle, *Phys. Rev. B*, 2007, **76**, 165202.
- 63 B. Cao, W. Cai and H. Zeng, *Appl. Phys. Lett.*, 2006, **88**, 161101.
- 64 Y. M. Sun, Ph.D. thesis, University of Science and Technology of China, July, 2000.
- 65 M. Willander, O. Nur, J. R. Sadaf, M. I. Qadir, S. Zaman, A. Zainelabdin, N. Bano and I. Hussain, *Materials*, 2010, **3**, 2643–2667.
- 66 P. S. Xu, Y. M. Sun, C. S. Shi, F. Q. Xu and H. B. Pan, *Nucl. Instr. and Meth. in Phys. Res. B*, 2003, **199**, 286–290.